

of fiber is produced. In the pultrusion technique shown in Figure 4, fibers are first pulled through a resin bath. Once the fibers are impregnated with resin, preformers create the shape of the final product. Finally, the impregnated fibers are pulled through a heated die which cures the matrix and gives the pultruded section its final shape. To allow for different diameter rebars to be fabricated using the same pultrusion machine, two steel plates between the heating elements were designed to accommodate 3/16 inch outside diameter to 3/8 inch outside diameter brass tubing to act as the actual die. The tubing could easily be removed from the steel plates for repair and/or replacement. Most commercially available FRP reinforcing products are produced using the pultrusion technique because of its economic process and minimal fiber waste.

Once the core is produced, a filament winding machine as shown in Figure 5 is used to symmetrically place additional fibers around the core. In this research, a computer controlled three axis filament winding machine was used to wind fibers around the core. A great advantage of any computer controlled filament winding machine is its ability to precisely apply fibers around a mandrel. Since symmetric fiber placement is desired, parameters such as the diameter of the core, the wind angle, and the bandwidth of the fibers used must be entered into the filament winding machine prior to winding. The wind angle is measured from the longitudinal axis of the core to an axis perpendicular to the core. Each fiber has its own bandwidth, or the width of a fiber tow when it is spread across the mandrel. The core is placed in the chucks of the headstock and tailstock axes, and as these two axes rotate in the same direction, a third axis applies fibers to the surface of the core. To achieve longitudinal strength and stiffness as required in FRP reinforcing,

filament wound fibers were placed with a low wind angle with respect to the longitudinal axis of the core. All filament wound rebars were cured at room temperature for a period of 48 hours.

The final hybrid FRP rebar consists of one type of fiber in the core, with two fibers symmetrically placed on the surface of the core. It is believed that symmetric fiber placement would eliminate any eccentric stress redistribution during fiber breakage.

In order to develop and transfer stresses in a reinforced concrete structure, a bond must exist between the reinforcing and concrete. There are two components of this bond in current mild steel reinforcing; frictional bond and bearing bond. Frictional bond relies on the adhesion of the reinforcing to the concrete. In other words, once the frictional bond is broken, there is no more bond. Developing stresses based on frictional bond alone would require a large rebar embedment length. Conversely, bearing bond is created through a mechanical interlock between the deformations of reinforcing and the surrounding concrete. For a bearing bond to fail, either the concrete must undergo splitting, or the deformations on the reinforcing must yield.

In FRP reinforcing, a conscious effort has been made to improve both the friction and bearing bond [15]. It has been shown that a large frictional component can be developed by simply sand coating FRP reinforcing. However, this frictional component does not provide adequate bond between the reinforcing and concrete. Once the frictional bond is broken, nothing prevents complete pullout of the reinforcing. Thus, a bearing bond must be incorporated into the FRP reinforcing to provide an adequate amount of bond. Many FRP manufacturers use filament winding to include some deformations on the surface of the reinforcing. Many studies have shown that this

method of providing deformations does not split the concrete; rather it shears the deformations off the FRP reinforcing and bearing bond is completely lost [15].

The proposed hybrid FRP rebar can easily be sand coated directly after the filament winding process by applying sand to the uncured matrix. In addition, deformations may also be incorporated to increase the bond characteristics. Shearing of the deformations may be eliminated by adjusting the wind angle and interweaving of the fibers that create the deformations, although this has yet to be proven. Since fibers have excellent longitudinal strength, a low wind angle would prevent shearing of the fibers from the rebar. In addition, if the deformations are built up, i.e., many fiber tows are used to create each deformation; this would give the deformations additional strength against shearing.

D. MATERIAL SELECTION

After using the rule of mixtures to develop a theoretical hybrid FRP stress strain relationship, fibers of different stiffnesses and failure strains were sought. Table I shows the materials selected and their corresponding volume fractions. All material properties for fibers and resin were provided by the manufacturers. Zoltek fibers were used in the core, while Mitsubishi fibers were filament wound around the core at an angle of 20 degrees. The wind angle was selected to provide adequate longitudinal strength. The Shell Epon 9500 resin system was mixed with Shell Epi-Cure Curing Agent 9550 at a ratio of 100 parts resin to 33 parts curing agent by volume. During the pultrusion process, 1 part release agent (MOLD WIZ INT-1846) was added to the matrix to prevent adhesion to the heated die.

To accurately develop a theoretical model, all filament wound fibers were adjusted to account for the wind angle. From the volume fractions in Table I, an initial stiffness of 20.7 Msi at a pseudo-yield strain of 0.003 was established. While the pseudo-yield stress at this point is slightly higher than that of mild steel reinforcing, it was determined that this pseudo-yield point would not be reached due to the shock wave phenomena reported by previous investigators [8,9].

Table I Specifications of Proposed Three-Fiber Hybrid Rebar

Fibers	Type	Volume Fraction %	Elastic Modulus (Msi)	Failure Strain in/in	Wind Angle (degrees)	Manufacture Technique
1	Mitsubishi K137HG	5%	131	0.003	20	Filament Winding
2	Mitsubishi K13710	12.5%	94	0.0045	20	Filament Winding
3	Zoltek Panex-33	19%	33	0.0159	0	Pultrusion
Matrix	Shell Epon 9500	63.50%	0.45	0.113	N/A	N/A

E. INTEGRATION OF FIBER OPTIC SENSORS

To incorporate fiber optic sensors inside the proposed hybrid FRP rebar, an intermediate step between pultrusion and filament winding was added. By securing the fiber optic sensor on the surface of the core, the fiber optic sensor was covered by the filament winding process. Complete coverage of the sensor by the filament wound fibers would protect the sensor from the harsh concrete environment. Furthermore, several fiber optic sensors may be placed within the same hybrid FRP rebar to measure strains in various locations along the structure without degradation of the hybrid FRP material

properties. Extreme care must be taken to ensure a reliable ingress/egress point of the fiber optic line. The fiber optic line can be damaged at this point thus rendering the sensor completely ineffective.

F. LIMITATIONS AND DRAWBACKS

There are some drawbacks to the proposed smart hybrid FRP rebar. The Shell Epon resin system is a thermoset resin; once the resin cures, there is no reshaping of the final product. Any thermoset resin system would prevent standard hooks or stirrups to be fabricated at the jobsite. However, this issue is easily resolved by selecting a thermoplastic resin system. In a thermoplastic resin system, localized reheating of the FRP would soften the matrix, allowing the reinforcement to be shaped.

Another limitation is the size of the filament winding machine. The proposed hybrid FRP rebars were fabricated using a Composite Machines Company filament winding machine with a usable mandrel (or core) length of 78 inches. In the future, if longer hybrid rebars are required a larger filament winding machine will be needed.

IV. FRP REBAR TENSILE TESTS AND RESULTS

A. GENERAL

The purpose of the tensile testing program was to determine if the theoretical investigation could accurately represent the material behavior of the proposed hybrid FRP rebars. From the theoretical investigation, a three fiber hybrid FRP rebar should exhibit three peaks, each peak signifying the rupture of one type of fiber. The results of these tensile tests were used in the design of the hybrid FRP reinforced concrete beams in Section V.

B. PREPARATION OF FRP REBAR COUPONS

Tensile testing was performed on each batch of hybrid FRP rebars to account for variations in the manufacturing process. From each batch, three tensile coupons were selected. A gage length of about 24 inches was chosen to allow for a reliable average strain measurement over the coupon.

Researchers have used various methods to test FRP rebars in tension. Malvar and Bish [16] provide a comprehensive overview of various gripping mechanisms. From their research, it was observed that the ASTM standard test method for tensile determination of FRP rebars produced the lowest strength values. In addition, failure at the grip/coupon interface usually resulted in lower strength values. It was determined that a clamp type grip with end wrapped specimens yielded the best results. The testing method and specimen preparation for the testing program was based on the results of [17].

Preliminary tensile testing of the proposed hybrid rebars revealed possible premature failure at the grip/coupon interface. In all preliminary testing, failure of the coupon occurred within the hydraulic grips. It was determined that the serrated edges of the grips crushed the ends of the coupon, thus causing a weak point in the coupon. This phenomenon does not occur in a steel coupon test because steel is isotropic and has equivalent strength in all directions. Furthermore, slippage between the grips and the coupon was also evident in some trial testing. To avoid premature failure at the grip/coupon interface, both ends of each coupon were filament wound with additional carbon fiber to a thickness of twice the rebar diameter. In addition, a hydraulic grip pressure was determined through a trial and error approach to eliminate crushing of the coupon. During some coupon tests, slippage sometimes occurred between the coupon and the filament wound wrap. This slippage was determined by inspecting the ends of the coupons after the test. If substantial slippage had occurred, results from that test were discarded and new coupons were prepared.

C. TESTING APPARATUS AND DATA ACQUISITION

All tensile testing of the proposed hybrid FRP was performed using a MTS Series 880 Universal Testing Machine. This machine uses hydraulic "V" notch type grips with serrated surfaces to test circular cross section specimens. A hydraulic grip pressure of 500 psi was selected to prevent crushing of the coupon while eliminating slippage between the grips and the filament wound ends of the coupon.

To determine the exact load deflection behavior of the proposed hybrid FRP, each tensile test was performed under displacement control at a rate of 0.039 in/minute. A

slow rate was selected to ensure all data collection during the test. For comparison, ASTM D3916-94 (Standard Test Method for Tensile Properties of Pultruded Glass-Fiber-Reinforced Plastic Rod) requires a crosshead speed rate of 0.2 in/minute for a displacement controlled tensile test. The applied load was measured using an internal load cell, while the crosshead motion was monitored by an internal linear variable differential transformer (LVDT). As mentioned in the previous section, after each test the coupon was checked for slippage in the grips. Observation of ends of the coupons would easily determine if slippage had occurred. If any slippage had occurred, the test data was discarded and a new coupon was tested. The test data was collected using a proprietary data acquisition program at a rate of 10 data points per second.

D. RESULTS OF TENSILE TESTS AND DISCUSSIONS

The primary objective of the tensile testing program was to determine if the theoretical stress-strain curve of a hybrid composite rebar could be reproduced through experimental testing. Figure 6 shows the theoretical stress strain curves based on the fiber volume fractions in Table I. There are three distinct peaks in Figure 6; each peak corresponds with the failure of one type of fiber. From the selected materials and volume fractions, this stress strain curve should theoretically provide gradual failure, or in other words the desired pseudo-ductility. The theoretical pseudo-yield point of this hybrid reinforcing occurs at a stress of 62,000 psi, with a pseudo-yield strain of 0.3 %.

Figure 7 compares the theoretical stress - strain curve with the experimental stress strain curve for a typical tensile test coupon fabricated following Table I. From the experimental stress strain results of three tests, an average stiffness of 13.8 Msi was

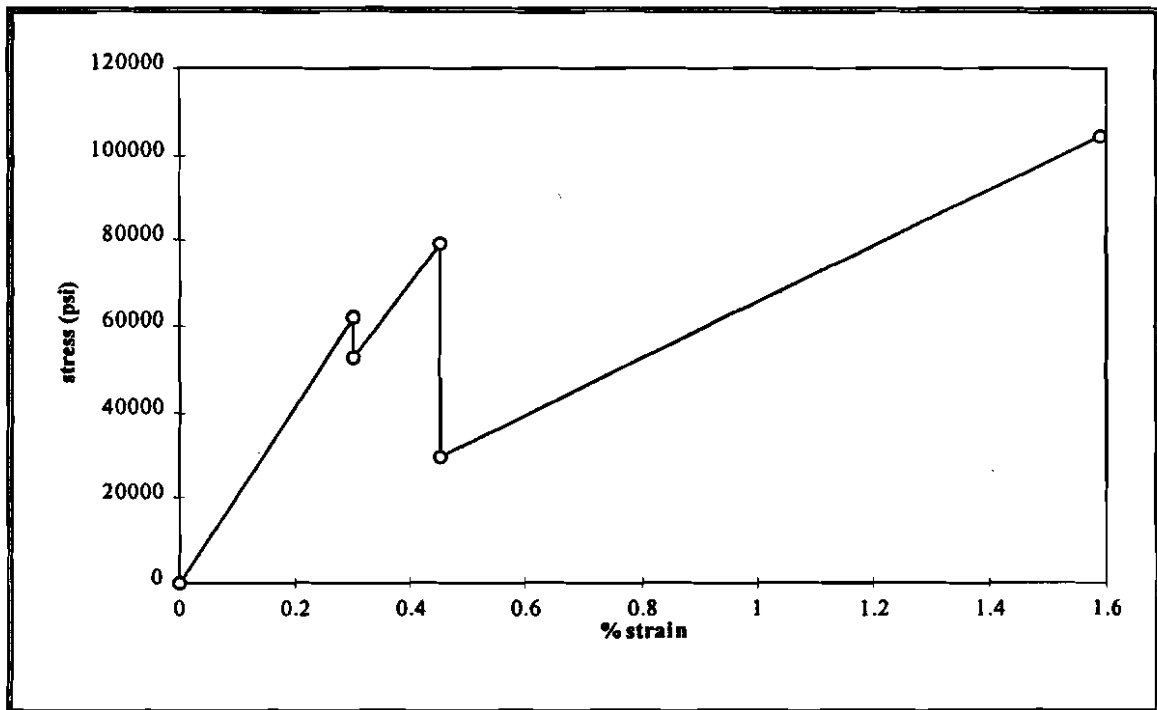


Figure 6 Theoretical Stress Strain Curve of 3-Fiber FRP

computed. The measured pseudo-yield stress was 56,600 psi, while the measured pseudo-yield strain was 0.41%. Under tension, the rebar coupons experienced successive cracking of the filament wound shell. Each crack corresponded with a drop in load, as shown in Figure 6. Furthermore, these cracks were spread out evenly across the gage length of the coupon at a crack spacing of 4 to 5 inches. Figure 8 represents a typical cracking sequence for the coupons tested. It was also observed that the load increased after the occurrence of each crack. Finally, the core ruptured at a strain comparable to that of the Zoltek carbon fibers used in the core.

It is shown in Figure 7 that the experimental stress - strain relationship does not correlate with the theoretical curve. In the experimental curves, five peaks occur during the load history of the coupon using only three different types of fibers. According to the

The same manufacturing process was used for these hybrid rebars: Zoltek fibers were used in the pultrusion process, while Mitsubishi K137HG fibers were wound around the core. Figure 10 shows the experimental stress - strain behavior of the two-fiber hybrid rebar. Under tension, multiple cracking of the shell was again observed, with a crack spacing between 2 to 3 inches. It is believed the crack spacing was smaller due to the lower failure strain of the filament wound shell. A total of seven cracks were observed during the test. However, some cracking must have occurred simultaneously because only four peaks are evident from Figure 10. A stiffness of 13.8 Msi was experimentally measured, with a pseudo yield strain of 0.31%. The pseudo yield strain observed corresponds with the failure strain of the Mitsubishi K137HG fibers; this agrees with the concrete stiffening concept. Application of the rule of mixtures would also determine a pseudo yield strain of 0.3%; however, the additional peaks until failure can only be explained with the concrete stiffening analogy mentioned above.

One more observation can be made from the experimental stress-strain relationships of both the two-fiber and three-fiber hybrid rebars. If the slopes of the corresponding peaks are extrapolated to the x-axis as shown in Figure 11, the slopes do not pass through the origin. Pseudo-permanent deformation has occurred in the hybrid rebar, due to the multiple cracks in the shell. Furthermore, if the stiffness of the peaks within the pseudo-ductile region are computed, the stiffness computed would be comparable with the initial stiffness before any cracking has occurred. This implies that if the proposed hybrid rebar was exposed to repeated loading, the hybrid rebar would perform similar to steel, although this is speculation at best since no repeated loading tests were performed. This observation is also contradictory to the assumption of the law

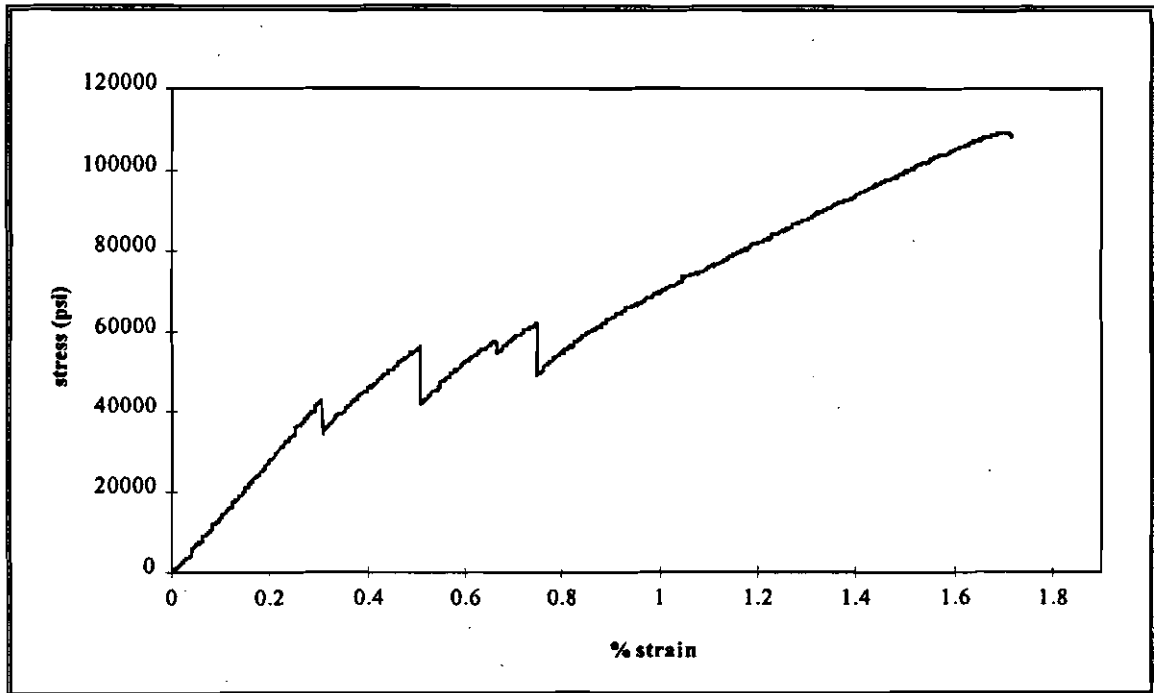


Figure 10 Experimental Stress Strain Curve for 2-Fiber FRP

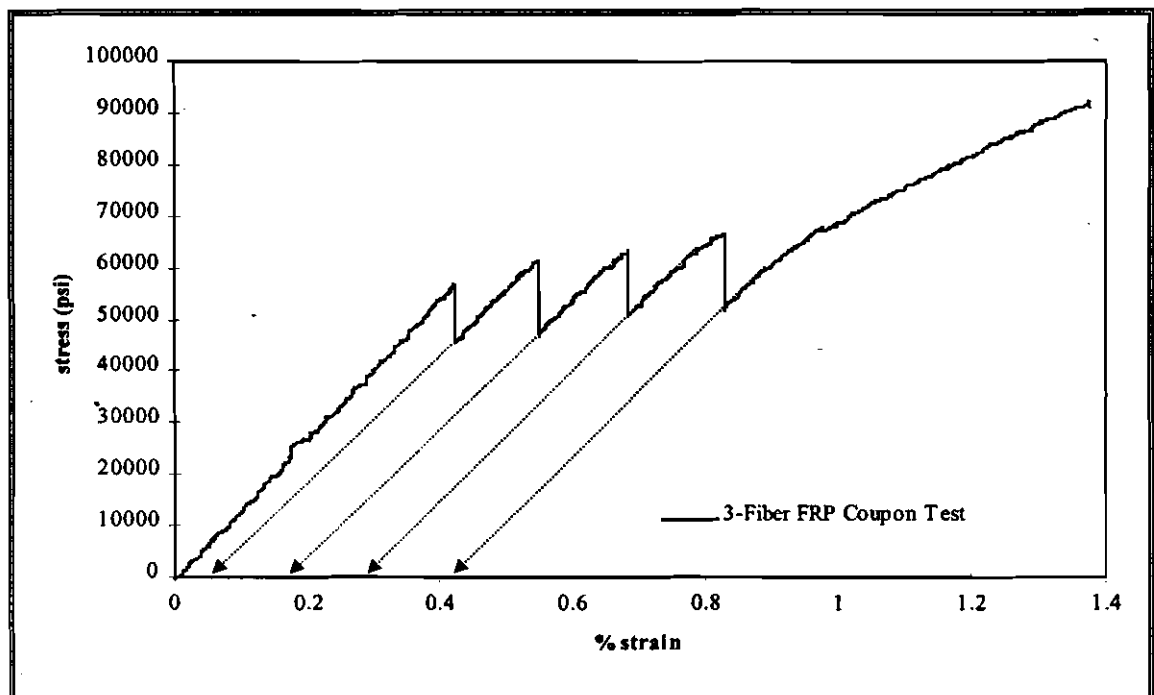


Figure 11 Extrapolation of Peak Slopes in Pseudo-Ductile Region

E. COMPARISON OF HYBRID FRP AND STEEL REINFORCING

of mixtures that residual strains do not exist but stiffnesses reduce after breakage of some fibers.

One of the objectives of this research was to develop a hybrid FRP rebar with comparable engineering properties to that of steel rebar. In this respect, Figure 12 compares the stress-strain curves of the proposed hybrid FRP with conventional Grade 40 and 60 mild steel rebars. Many deficiencies are evident, beginning with the stiffness of the hybrid FRP. The initial stiffness of the hybrid FRP is approximately half when compared to mild steel rebar. This indicates a hybrid FRP reinforced structure will have larger service load deflections as compared to a steel reinforced structure. Another deficiency is the pseudo-yielding plateau of the proposed hybrid FRP. While the small pseudo-yield plateau looks negligible when compared to the steel yielding plateau, this is quite misleading. In some steel reinforced concrete structures, the full yielding region of steel is never fully utilized. Therefore, there is additional ductility that is not used in steel rebar because crushing of the concrete occurs before the strain hardening region is entered. Consequently, the proposed hybrid FRP rebar has adequate pseudo-ductility and a pseudo-strain hardening region for use in reinforced concrete design as shown in the beam test results in Section V.

F. DRAWBACKS IN THE MANUFACTURE OF THE PROPOSED HYBRID FRP

With more experience in the manufacturing techniques of the proposed hybrid FRP system, a suitable corrosion free replacement for mild steel rebars will be possible in the future. From the previous section, three engineering properties require improvement: the initial stiffness, the pseudo-ductile region, and the ultimate strain.

a custom matrix resin application system is designed for use with the filament winding machine, difficulties will always exist in controlling the fiber volume fraction of any filament wound rebar.

The ultimate strain and pseudo-ductile region are related in that the stiffer the core material is, the smaller the pseudo-ductile region will be. In the future, a hybrid FRP rebar should be fabricated with a pultruded core consisting of a large failure strain fiber such as Kevlar-49, and a filament wound shell consisting of Mitsubishi K137HG. With these fibers, a large pseudo-ductile region and a large failure strain should be observed. Furthermore, the slope of the pseudo-strain hardening region will be reduced thus making it more comparable to the slope of the strain-hardening region in mild steel.

G. CONCLUDING REMARKS

Even though the theoretical investigation does not correlate with the experimental results, pseudo-ductility in the proposed hybrid FRP rebars was achieved. The concrete stiffening concept can be used to explain the experimental results with relative confidence. Furthermore, by placing fibers symmetrically over the cross section of the rebar, eccentric stress redistribution during fiber breakage was eliminated. Additional testing will be carried out in the future to address the issue of slippage at the grip/coupon interface, or mismeasurement of the deformation of the coupon.

There are some shortcomings in the material behavior of the proposed hybrid FRP as well. As mentioned earlier, carbon fibers reach their stiffness at very high stress levels. To achieve a material behavior similar to mild steel reinforcing, the stiffness must be achieved at a relatively low stress. The proposed hybrid FRP reinforcing does not

V. FLEXURAL TESTING OF R/C BEAMS AND RESULTS

A. GENERAL

To investigate the ductile behavior of the proposed hybrid FRP rebars embedded in concrete, a flexural testing program was performed. The study consisted of six reinforced concrete beams having different types of reinforcement. Two beams consisted of different percentages of steel reinforcing, while three beams were designed with the proposed hybrid FRP rebars. A final beam was designed using unidirectional FRP reinforcing. Monotonic as well as repeated loading tests were performed.

The goal of the flexural testing program was to collect data to compare the behavior of the hybrid FRP reinforced beams with the steel and unidirectional FRP reinforced beams. The comparisons made will help determine if the proposed hybrid FRP system will be a viable corrosion free alternative to steel in the future.

B. THE TEST BEAMS

In order to examine the flexural capacity of a reinforced concrete beam, the overall dimensions of the beam are critical. To accurately test the flexural capacity in a test beam, the shear component should be minimized so that the flexural component can be observed. The shear span to depth ratio of a given beam can provide information to help determine which component dominates the behavior. For example, a beam designed with a shear span to depth ratio less than or equal to 2.5 typically has a large shear component; many different failure modes are observed in the behavior. A testing program should be conceived in such a way that one type of failure mode is forced upon

all the specimens so that comparisons between the different specimens can be made. Thus, a beam designed with a small shear span to depth ratio would not provide representative flexural capacity results. On the other hand, if a shear span to depth ratio between 2.5 and 6 is selected, the shear contribution is not as great, and thus representative flexural capacity results may be obtained.

In this testing program, the overall length of the beams was limited to the length of the hybrid FRP rebars. As mentioned earlier, the proposed hybrid FRP rebars were fabricated using a filament winding machine with a usable mandrel (or core) length of 78 inches. Therefore, the overall length of the test beams was predetermined at 78 inches. Then, to force a flexural failure mode, a shear span to depth ratio greater than 2.5 was selected for a preliminary beam design. A four point bending test was also used to achieve a shear span to depth ratio greater than 2.5 A summary of beam dimensions,

Table III Summary of Beams

Beam	Reinforcing Type	f_c (psi)	Curing Time, days	b (in)	d (in)	A_s (in ²)	ρ
1S1.0	Steel	5500	21	4.75	6.75	0.33	1.0
1FRP1.0	Hybrid FRP	5500	22	4.75	6.75	0.2886	0.9
2FRP1.0R	Hybrid FRP	5500	23	4.75	6.75	0.2886	0.9
2S1.7R	Steel	5500	20	4.75	6.75	0.55	1.7
3FRP1.5	Hybrid FRP	5100	15	4.75	6.75	0.481	1.5
4FRP0.5	Unidirectional	5500	19	4.75	6.75	0.1657	0.5
3S2.0	Steel	4500	28	4.75	6.75	.66	2.0
5FRP1.8	FOS Hybrid FRP	4500	28	4.75	6.75	0.58	1.8
5FRP1.8	FOS Hybrid FRP	4500	28	4.75	6.75	0.58	1.8

concrete strength, and reinforcing percentage is shown in Table III. Beams designated with an "R" signify a repeated loading test, while all other beams underwent monotonic loading until failure. Two beams (5FRP1.8 and 5FRP1.8) were instrumented with fiber optic sensors.

Since the objective of this testing program requires a flexural failure mode in the test beams, all shear reinforcing according to ACI 318-95 was over-designed to prevent any type of shear failure mode. For all test beams, shear reinforcing was fabricated from #3 Grade 40 mild steel reinforcing bars. Figure 13 shows the locations of all shear reinforcing as well as the support and load points.

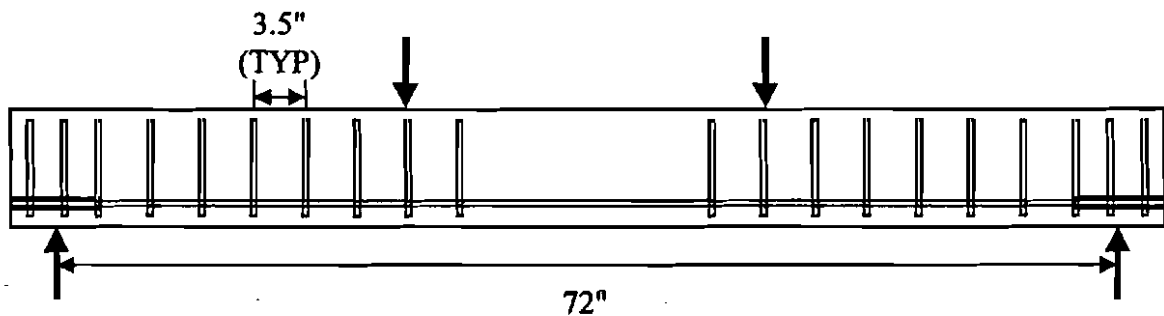


Figure 13 Typical Stirrup Placement

C. MATERIALS

1. Concrete. The concrete used in all the test beams was designed to achieve a 14 day compressive strength of 4000 psi. The material quantities for each batch are shown in Table IV:

concrete. All composite rebars were fabricated in the Composite Manufacturing Facility at the University of Missouri - Rolla.

D. DESIGN AND OBJECTIVES OF TESTS

The objective of the testing program was to compare the behavior of different types and percentages of reinforcing under flexure. One method to compare the behavior of different beams is to measure the curvature of each test beam as well as the midspan deflection. Comparisons can then be made between the theoretical approach and experimental test data as well as between different types of reinforced beams.

All beams were designed as under-reinforced beams according to the ultimate strength design approach [18]. In the ultimate strength design approach, a strain compatibility diagram is used to find the relationship between the concrete strain and the reinforcing strain using similar triangles, as shown in Figure 14. If the stress strain relationships of both the concrete and the reinforcing are known, a stress diagram is then produced. Once a stress diagram is established, equilibrium of forces and moments is applied to determine the flexural capacity of the cross section.

To simplify computations and to follow the American Concrete Institute Building Code 318-95, the parabolic compressive stress diagram of concrete was converted to an equivalent stress block using the Whitney's equivalent stress block approach. In the Whitney's stress block approach, the variables α and β_1 are computed to give an equal area when compared to the parabolic stress diagram. Also, the α and β_1 values computed account for the locations of the centroids of both the parabola and the rectangular stress

4.46% is computed. This is a well established equation printed in all reinforced concrete design textbooks.

Since the proposed hybrid FRP rebar does not have engineering properties similar to steel reinforcing, a new equation to determine the balanced condition must be derived so that an under-reinforced hybrid FRP concrete structure can be designed. Equation 6 represents the balanced condition based on the engineering properties of the hybrid FRP rebar:

$$\rho_b = \frac{0.85\beta_1 f'_c}{f_y} \left(\frac{40500}{40500 + f_y} \right) = \frac{A_s}{bd} \quad (6)$$

Using a pseudo-yield stress of 56,500 psi and a concrete stress of 5,500 psi, a ρ_b of 2.76% is computed from Equation 6.

In comparing the percentage reinforcing of each test beam [Table III] with respect to the balanced conditions computed above, all test beams have been designed as under-reinforced beams. Ductile failure should be observed in all test beams with the exception of the unidirectional FRP reinforced beam. Since unidirectional FRP reinforcing has no yield plateau, a brittle failure is expected.

One method to compare the behavior of different reinforced concrete beams is to compute moments and curvatures. To develop moment curvature diagrams for a given cross section, a concrete strain is first selected. From this concrete strain, the corresponding reinforcing strain is determined through the strain compatibility. This step is required to determine if the reinforcing has reached its yield or pseudo-yield point.

Once this has been established, the moment capacity at the given concrete strain is computed by summing moments about the location of the reinforcing:

$$M = \alpha\beta_1 f'_c bc \left(d - \frac{\beta_1 c}{2} \right) \quad (7)$$

In addition, the curvature at the concrete strain must also be computed. The equation for the curvature at a given concrete strain is :

$$\phi = \frac{M}{EI} = \frac{\epsilon_c}{c} \quad (8)$$

The curvature represents the reduction of the moment of inertia for a given reinforced concrete cross section. This is an important measure of the ductility of a cross section. Before cracking of the concrete, the moment of inertia is the greatest and the curvature is small since the entire cross section is effective. As tensile cracks begin to occur, the curvature increases due to an increase in the concrete strain and the upward movement of the neutral axis. The end result is a reduced effective moment of inertia since all concrete below the neutral axis becomes ineffective due to cracking.

To develop moment curvature diagrams for a specific cross section, a minimum of four points are required to reflect changes in the material behavior: cracking of the concrete, yielding (or pseudo-yielding) of the reinforcing, strain hardening (or pseudo-strain hardening) of the reinforcing, and the point at which concrete crushes. The

contribution of concrete before cracking was also considered in this study. These four points make up the general moment curvature diagram.

Once these points are determined, a load deflection curve can be constructed for any location on the beam. The double integration method was applied to determine the load deflection curves at midspan for all beams. In this method the curvatures are applied as distributed loads on the test beam. The deflection at midspan of the actual beam can then be computed by integrating the curvatures twice over the test beam.

E. TEST SETUP AND DATA ACQUISITION

All beams were tested using a MTS Series 880 Universal Testing Machine. The MTS machine was modified with compression platens and a seven foot long W section steel beam to accommodate flexural testing of the reinforced concrete beams, as shown in Figure 13. Each beam was simply supported using pin and roller supports clamped to the W section. For the purpose of safety and lateral restraint, two wooden frames were attached with bolts to the W section. If any lateral movement was encountered during a test, the wooden frames would prevent any lateral movement until the test was terminated.

As mentioned earlier, standard hooks were used in the steel reinforced concrete beams to develop stresses. The hybrid FRP and unidirectional FRP rebars were sand coated in addition to being filament wound at the ends to provide some bearing capacity. To prevent longitudinal splitting of the concrete at the ends of the FRP reinforced beams (and subsequent pullout of the reinforcing), steel plates were clamped around the outside

of the beams at the support locations to provide confinement of the concrete. This approach proved, since none of the FRP reinforced beams exhibited pullout of the reinforcing.

Monotonic and repeated loading tests were performed on various test beams. To allow comparisons between repeated loading tests and monotonic tests, the envelopes of the repeated loading tests were determined by eliminating all load/unload data points. Load was applied at quarter points along the test beam using pin and roller supports, as shown in Figure 15. All monotonic tests were performed under displacement control at a rate of 0.0394 in/min. Repeated loading tests were also performed under displacement control at a loading rate of 0.0394 in/min, but an unloading rate of 0.197 in/min was used in the interest of time. Slow displacement rates were selected to ensure enough data collection during the test. Furthermore, unloading during a repeated loading test occurred when the midspan deflection of the test beam reached multiples of 0.12 inches. A stipulation of this type allowed for comparisons between the steel reinforced test beam and the hybrid FRP reinforced test beam.

The data collection was made using six linear variable differential transformers (LVDT), an MTS internal load cell, two dial gages, and a data acquisition system (Labtech). LVDT placement on the test beams are summarized in Table V.

within the constant moment region, while an 18 inch gage length was chosen to ensure an average strain value reading. From the strain diagram, the location of the neutral axis was determined and the concrete compressive strain was computed using similar triangles. The curvature was then computed using Equation 8. To determine the corresponding moment at the measured strains, appropriate α and β_1 values were selected and Equation 7 was finally used to compute the moment capacity. Experimental and theoretical moment curvature diagrams are presented in the following section.

Midspan deflection was measured using LVDT #5 and #6. Since a direct measurement of deflection was performed, no calculations were required to compare the experimental results with the theoretical results. However, the stiffness of the beam test setup did affect the LVDT measurements. To account for the stiffness of the beam test setup, dial gages were placed to measure the deflection of the W section at the location of the test beam supports. Dial gage readings were recorded at different load stages, and a linear relationship between load and deflection was established. All theoretical load deflection curves were adjusted to account for this relationship so that a direct comparison between the theoretical and experimental load deflection curves could be made. These comparisons are presented in the following section.

All LVDTs and the MTS internal load cell were calibrated for use with the Labtech data acquisition program. During testing, Labtech was programmed to continuously collect data at a rate of one data point per two seconds for all LVDTs and the load cell.

F. RESULTS OF FLEXURAL TESTS AND DISCUSSIONS

The objective of the flexural testing program was to compare the behavior of various types and percentages of reinforced concrete beams. Theoretical and experimental moment curvature diagrams for each test beam along with the load deflection curves for each test beam will be used to evaluate the behavior of each beam. These comparisons will be beneficial in determining the future of the proposed hybrid FRP rebars.

1. Theoretical vs. Experimental Moment Curvature Diagrams. As discussed in previous sections, curvatures for each test beam were computed from the LVDT strain measurements. From similar triangles, strain measurements at the extreme concrete compression face and at the location of reinforcing were computed along with the location of the neutral axis. In addition, the experimental moments were computed from the experimental strain diagram. Therefore, all components of the experimental moment curvature diagrams were computed from strain compatibility.

The moment curvature diagrams of beam 1FRP1.0 are shown in Figure 16. Both the pseudo-yielding curvature and the ultimate curvature correlate well with the theoretical values. Furthermore, since moments were computed from the curvatures, the instrumentation of this beam accurately measured the experimental behavior.

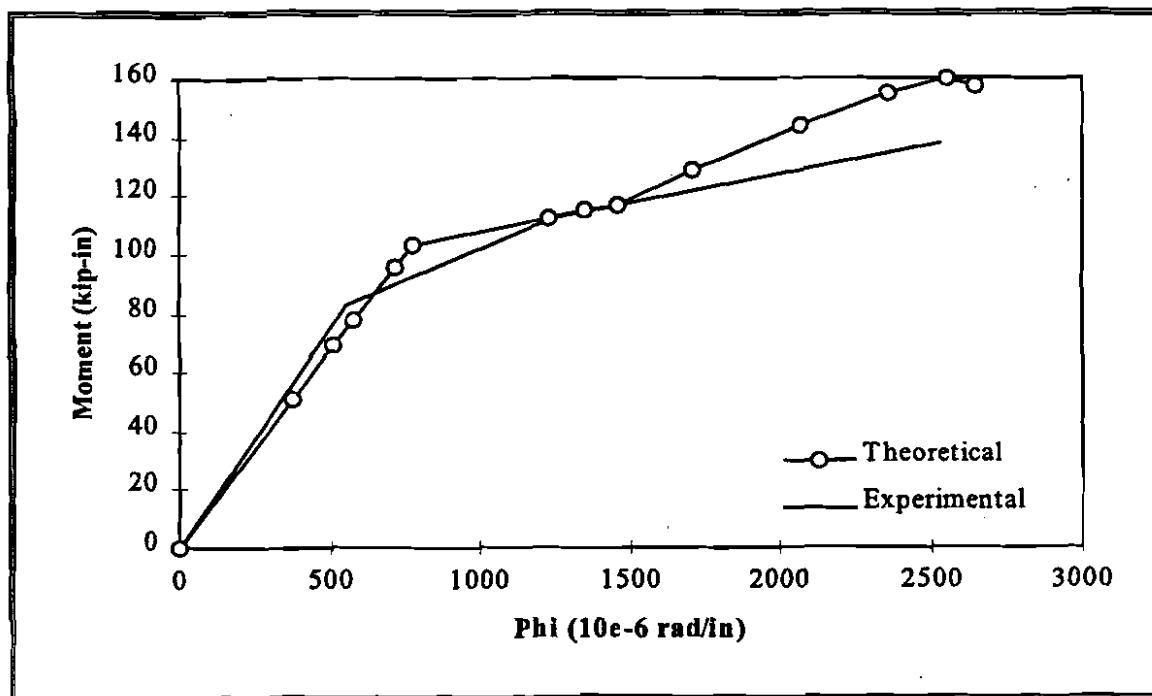


Figure 16 Beam 1FRP1.0 Moment Curvature Diagrams

The experimental moment curvature diagram for beam 3FRP1.5 did not correlate well with the theoretical. From the raw data, it was observed that the compression LVDTs did not accurately measure the compression strain. After testing, it was determined that both compression LVDTs were not instrumented properly; the connections between the LVDT and the mounting stud were such that small changes in the strain were inaccurately measured, as shown in Figure 17. A gap existed between the LVDT and the mounting stud which resulted in no strain readings until the gap was closed. By measuring less compressive strain, the neutral axis location was determined to be closer to the top of the beam than the theoretical neutral axis. The end result was an overestimation of the curvature and an underestimation of the moment capacity at a given curvature.

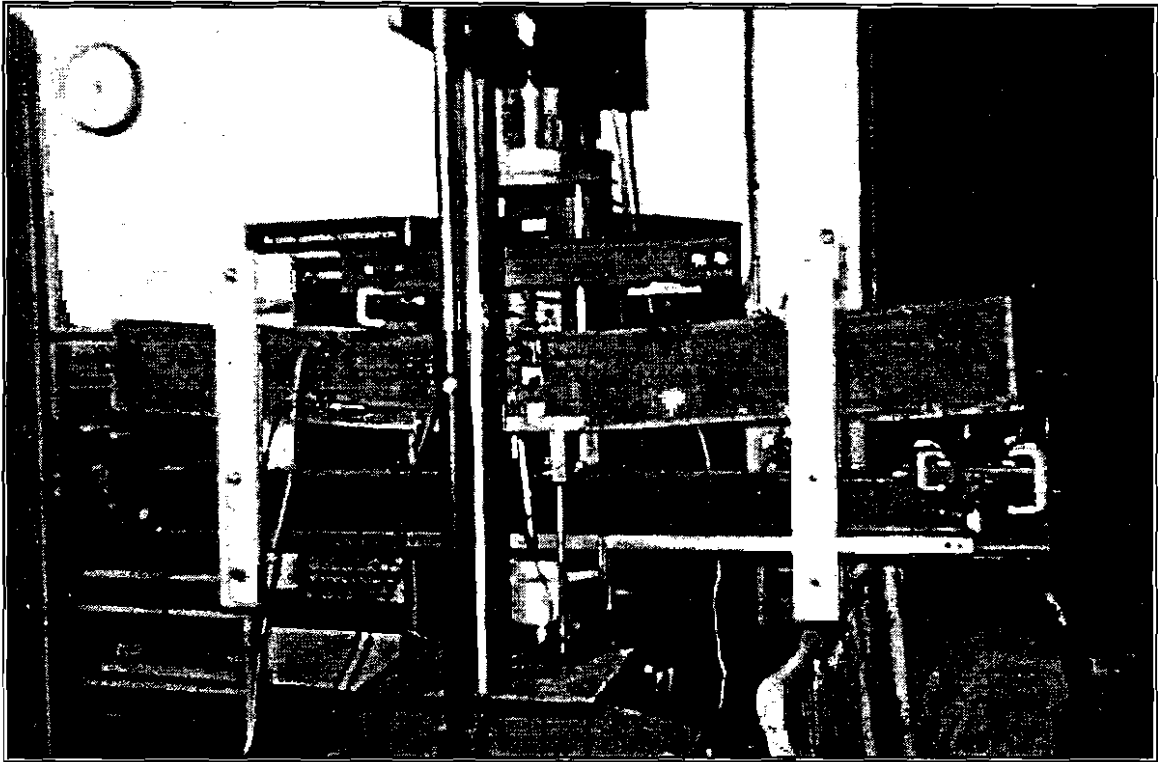


Figure 26 Beam 3FRP1.5 Ductile Failure

It is obvious that an allowable stress design approach should be imposed on unidirectional FRP rebars to account for the lack of ductility in the cross section. By providing an allowable stress limit, additional capacity is exchanged for the lack of ductility. Nonetheless, a brittle failure mode will occur with unidirectional FRP rebars, regardless of the allowable stress limit imposed.

As important as it is to theoretically determine the behavior of a reinforced concrete beam, it is also vital to present comparisons between different types of reinforcing. Figure 28 represents the experimental load deflection curves for beams 1S1.0 and 1FRP1.0. Ductility is evident in the hybrid FRP reinforced beam when

G. DUCTILITY INDEX

Since ductility is measured beyond the yield point of reinforcing in a concrete structure, energy methods can be useful to help describe the behavior of the structure. Any energy method usually requires an approximation or numerical integration of the area underneath a curve. The computed area is considered the energy absorbed by the system. For a ductile structure this area will be large, but for a brittle structure this area will be considerably less. In this study, the load deflection curves were used to determine the energy of the test beams. Naaman and Jeong [20] define a ductility index based on the energy computed from load deflection curves:

$$\mu_w = \frac{1}{2} \left(\frac{W_{\text{tot}}}{W_{\text{el}}} + 1 \right) \quad (9)$$

where W_{tot} is the energy computed up to failure, and W_{el} is the energy computed for the elastic portion of the load deflection curve. This allows direct comparisons of ductility between test beams regardless of their material and geometric properties.

In addition to ductility based on energy, another measure of ductility can be computed from the load deflection curves. The ductility based on deflections follows Equation 10:

$$\mu_{\Delta} = \frac{\Delta_u}{\Delta_y} \quad (10)$$

where Δ_u is the ultimate deflection and Δ_y is the yielding deflection.

structures and the ability to be multiplexed [21,22]. The technology allows the measurement of internal strains and has the potential for long-term monitoring. A smart FRP rebar can give quantitative assessment of internal loading and damage. In this study, fiber optic sensors were placed inside FRP rebars, which in turn were placed in concrete beams. The sensors monitored strain during load tests and indicated the cracking events and the subsequent redistribution of load in the rebar.

Extrinsic Fabry-Perot interferometric (EFPI) single-mode fiber optic sensors were used to measure strain in FRP rebars [7]. These sensors were incorporated in the mid-length of the rebars during fabrication and were located between the pultruded core and the helical windings. The optical fiber lead for the sensors exited one end of the rebars through a protective plastic tube. The tube extended about a centimeter inside the rebar. The sensors were 250 micrometers in diameter and had a negligible effect on the rebar structure [23].

EFPI sensors consist of two glass fiber wave-guides inserted in a low-profile glass capillary tube. The end faces of the inserted fibers form a small cavity and are polished and coated for high reflectivity. Optical interference between reflections from the end faces is dependent on the cavity size. Longitudinal strain of the capillary tube induces a nonlinear optical interference signal. The operation of the sensors is described in the literature [22]. These sensors are environmentally rugged, are immune to electrical interference, are highly sensitive, and are compatible with FRP structures.

The optical sensors and instrumentation, in this study, were manufactured by Fiber and Sensor (F&S) Technologies. FOSS models were used with an optical wavelength of 1310 nm. Three EFPI sensors were numbered # 1, #2, and #3 and had gauge lengths of 4.66 mm, 5.01 mm, and 4.89 mm, respectively. They were demodulated using a fringe counting technique with strain resolutions of 35 $\mu\epsilon$, 33 $\mu\epsilon$, and 33 $\mu\epsilon$, respectively [7]. The instrumentation consisted of a laser diode optical source, a 3 dB fiber bi-directional coupler, and a high speed photodetector. The modulated optical

irregularity in the surface providing semi-rib texture. In addition, the surface is sand-coated to enhance the frictional force component.

The study of bond of particular reinforcement type can be very comprehensive by including the investigation of so many parameters such as, rebar type, rebar, size, embedment length, concrete strength, loading rate, etc. The scope of this study was limited and the objective was to provide a qualitative information about the FRP rebar characteristics as compared to steel rebars. All the FRP rebars produced for this study have a size comparable to number 3 steel rebars and a pseudo-yield stress comparable to grade 40 steel. Therefore, the study focussed on quantitatively determine the bond stress of both FRP rebars and companion steel rebar and compare the results based on bond strength and failure modes and draw conclusions and make recommendations.

1. Test Specimens and Materials. Twenty-four coupons were tested for bond characteristics (see Table VII). All test were pullout of rebars embedded in with embedment lengths were chosen to be 3 i. And 6 in. Nominal bond strength, slip at the onset of failure, mode of failure, and nominal bond stress-slip relationships were obtained from pullout tests of FRP rebars, and they were compared to pullout tests for steel rebars. The specimens were prepared using 6x12 inch steel cylinders. Before rebar placement the molds were cleaned and oiled. The rebar was placed axisymmetrically in the molds. Steel rebars and FRP rebars were used with length of four feet to provide ample length for gripping during testing. A list of the specimens included in this study are shown in Table VII. Two concrete strengths namely 5500-psi and 9000-psi were included. Rebar embedment lengths were 3 in. and 6 in. FRP rebars were manufactured with shell that consist of one round of filament winding (specimens 1-3xx and 1-6xx), two rounds of filament winding (specimens 2-3xx and 2-6xx) and some rebars with the

surface being sand coated (specimens 1-3s, 1-6s, 2-6s). All steel rebar specimens were labeled s-XX.

During the making of test specimen the rebars were restrained at both ends to keep the bars from moving during the pouring of the cylinders. To accomplish this a $\frac{3}{4}$ in x $1\frac{1}{2}$ in block of wood was placed in the bottom of the mold. This block had a hole in the center, sized to accept a length of PVC pipe. The pipe was placed on the end of the bars and sealed with silicone to adjust the embedment length as shown in Figures 35 and 36. A wood rack was built and placed over the molds to hold the rebar at the top as shown in Figure 37. This preparation was done 24 hours prior to the pouring of the specimens to provide time for the silicone seal to dry.

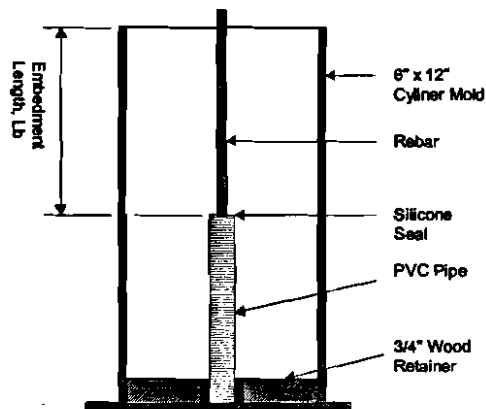


Figure 35 Side View of the Mold Setup

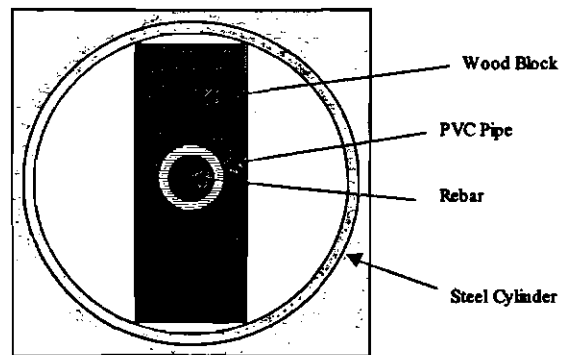


Figure 36 Top View of the Mold Setup

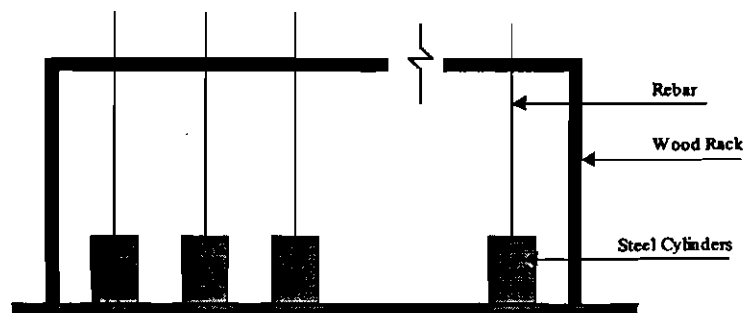


Figure 37 Drawing of the Rack Used to Hold the rebar Vertical During Pouring

2. Test Setup. The testing was performed at least 28 days after the pouring of the specimens. The test was set up as shown in Figure 38. The specimen was placed on top of a universal testing machine and resting on a $\frac{1}{2}$ inch thick bearing plate. The plates used for all rebars had a $1\frac{1}{2}$ inch hole in it. The rebar extended down and was gripped below. Two LVDTs of 0.001 inch range were placed at each end of the rebar to measure the slip occurring during the testing.

force divided by the nominal cross section of the rebar,. The values of the nominal bond stress were calculated by dividing the same recorded pullout force divided by the surface area of the bar embedded in the cylinder. For slippage, it was most logical to use the displacement measurements of LVDT 4, which actually recorded the movement of the bottom of the rebar inside the cylinder, as the total slip. In comparison to other methods that have been used to measure total slippage, this value was compared to the total displacement of LVDT 3, placed 8 inches from the top of the concrete, minus the actual elongation of the rebar recorded by the extensometer.

When comparing the bond stress of all specimens as shown in Table VII, results reveal that FRP rebars provide slightly less bond resistance as compared to steel bar. The maximum nominal bond stress is determined only when the rebar pulls out of concrete. If a rebar yield without pullout, the corresponding bond stress is not necessarily the bond resistance of that particular reb, such as the case of specimens s-6a and s-6b. Most of the FRP rebars did reach their pseudo-yield stress before pull out. This indicates that the bond stress recorded during tests are not the maximum bond stresses. Having used smaller embedment lengths would have resulted in higher bond stresses. The difference in mode of failures between steel rebars and FRP rebars is mainly observed in the post yield region. When the steel rebar yield, it continues to deform without pullout, however, the FRP rebar may end up with pullout just after the first yield (or crack of the shell). All the pullouts noticed in FRP beams were due to the pullout of the core from the shell after some cracking of the shell. However the shell maintained its adherence to concrete. This phenomenon was not observed in the beam tests since the rebars did not have free ends. FRP shell, in beams, continued to crack at concrete crack locations. Out of all the tests carried in this study, two of the specimens failed at the grip, the others all pulled

out of the concrete. Overall, the FRP rebars exhibited adequate bond resistance, especially, the sand coated rebars. The lack of bond was more at the core-shell interface rather than concrete-rebar interface. However, all bond damage of the core-shell interface occurred after pseudo-yield of the FRP rebars.

TABLE VII Summary of Bond Test results

Specimen Name See above	Concrete compressive strength f_c (psi)	Embedment length (in)	MAX Load (lbs)	Maximum Normal stress (psi)	Maximum Nominal Bond Stress (psi)	Measured total deformation outside cylinder (LVDT3) (in.)	Measured Total slip inside cylinder (LVDT4) (in.)
s-3a	6136	3	5811	52640	1645	.385	.354
s-3b	6136	3	6043	54742	1711	.351	.136
s-3c	9000	3	5329	48274	1506	.057	0
s-6a	6136	6	6956	63013	985	.39	.02
s-6b	6136	6	6973	63167	987	.342	.017
s-6c	9000	6	5230	47377	740	.115	.002
1-3a	5271	3	4283	38799	1212	.218	.349
1-3b	5271	3	4765	43165	1349	.19	.186
1-3sa	5271	3	4997	45267	1415	.055	.176
1-3sb	6136	3	4482	40601	1269	.021	.03
1-3sc	9000	3	6375	57750	1805	.184	.237
1-6a	5271	6	5346	48428	756	.109	.208
1-6b	5271	6	6060	54896	858	.835	.44
1-6sa	5271	6	3320	30075	467	.067	.002
1-6sb	9000	6	6259	56699	886	.438	.242
1-6sc	9000	6	5545	50231	785	.231	.535
1-6sd	9000	6	7072	64063	1001	.019	.001
2-6a	5271	6	6823	61808	966	.94	.668
2-6b	6136	6	5014	45420	710	.385	.009
2-6sa	5271	6	7288	66020	1032	1.148	.621
2-6sb	6136	6	4416	40003	625	.189	.351
2-6sc	9000	6	6541	59253	926	.992	.489
2-6sd	9000	6	5960	53990	844	.917	.599
2-6se	9000	6	5761	52187	815	.52	.129

J. CONCLUDING REMARKS

The beam testing program was successful in proving the pseudo-ductility of the proposed hybrid FRP rebars embedded in concrete. Excellent agreements with theoretical curves were obtained for all experimental load deflection curves. However, faulty instrumentation of some of the test beams prevented the experimental moment curvature diagrams to exhibit similar agreements with theoretical diagrams.

Furthermore, the advantages of structural health monitoring by using fiber optic sensors embedded within the hybrid FRP rebars has been demonstrated through the preliminary fiber optic sensor testing program. The sand-coated rebars also showed adequate bond resistance.

4. Ductility Index. Two different computations of ductility establish the pseudo-ductility evident in the proposed hybrid FRP rebars. It was also proven that currently available unidirectional FRP reinforcing does not provide ductility after post-yielding; thus a requirement of an allowable stress approach for current FRP is required.

5. Health Monitoring. The EFPI optical strain sensors survived the rebar and beam fabrication steps and operated during most of the load tests. The optical sensors did not fail until severe cracking of the concrete beam and the FRP rebar. The sensor data reliably indicated the occurrence of cracks and the subsequent redistribution of load in the rebar. The sensors reflected the different strain conditions in rebar at different locations in the concrete beam. The study demonstrated the usefulness of fiber optic sensors for monitoring internal strain in reinforced concrete subject to large. Furthermore, the advantages of structural health monitoring by using fiber optic sensors embedded within the hybrid FRP rebars has been demonstrated through the preliminary fiber optic sensor testing program.

6. Bond Resistance. The FRP rebars exhibited adequate bond resistance at the concrete-rebar interface. Bond stresses were comparable to those of companion steel coupons. Furthermore, all FRP rebars failed by yielding before pullout and the pullout occurred at the core-shell interface, which showed that bond failure may occur in the rebar itself that at the concrete surface.

23. A. M. Vengsarker, K.A. Murphy, and M. F. Gunther, "Low Profile Fibers for Embedded Smart Structures Applications," Proceedings of SPIE, 2360, pp. 372-375 (1994).